Supplementary Information

The extracellular chaperone clusterin sequesters oligomers of the Aβ$_{1-40}$ peptide

Priyanka Narayan, Angel Orte, Richard W. Clarke, Benedetta Bolognesi, Sharon Hook, Kristina A. Ganzinger, Sarah Meehan, Mark R. Wilson*, Christopher M. Dobson*, David Klenerman*

CONTENTS

<u>Supplementary Methods</u>

I.   Instrumentation and data acquisition

Further details on cTCCD instrumentation

With respect to the cTCCD detection, the measured blue to red channel cross-talk was 1% while crosstalk in the opposite direction was negligible. The dark counts on the detectors were found to be negligible as well.

The alignment and overlap of the laser beams was confirmed using a 40 base-pair dually labeled duplex DNA with one strand labeled with an AlexaFluor488 fluorophore and the other with an AlexaFluor647 fluorophore. Since this DNA sample is expected to have 100% association, measuring the association of the sample provides a measurement of the detection efficiency of the instrument. The maximum beam overlap was calculated to be ~30% using cross-correlation spectroscopy and the probe volume size was found to be 0.34 fL[45]. However, due to additional variation intensity of the lasers over the probe volume and fluorophores in untraceable dark states, the maximum detectable association was only ~25%.

The cTCCD instrument has a scanning stage which combines a Nikon Eclipse TE2000U microscope stage with two orthogonal DC motors (M-112.1DG, Physik Instrumente) to move it in the X-Y plane. The scanning speed of 200 μm s^{-1} was verified by test experiments with the DNA control sample not to detrimentally affect data acquisition for single pairs of fluorophores in either channel. The scanning starts at the top left-hand corner of the sample area and proceeds in a zigzag pattern across the sample area, triggering the MCS cards as it proceeds. The motors were programmed to trigger data acquisition only when a constant speed of 200 μm s^{-1} could be guaranteed for the entire frame (8 s) of data. For example, at either edge of the sample area data acquisition was not triggered until after motor deceleration and re-acceleration.

Further details on TIRFM instrumentation

To achieve good image registration, a grid consisting of regularly spaced ion-beam-etched holes in gold-on-glass was utilized. Dual-View[TM] optics were adjusted so as to maximize the overlap between red and blue images of the grid under white-light illumination resulting in measured image registrations in the range of ~75 nm.

The laser power used for taking measurements was 0.65 mW for the 633 nm channel and 0.14 mW for the 488 nm (as measured by epifluorescence at the sample plane) over an area of ~28 μm. Images were taken as averages of 30 frames of 100 ms each.

cTCCD and TIRFM sample acquisition

cTCCD time-course data for both aggregation and disaggregation experiments was acquired by taking a 1 μL sample from the solution and diluting it to a concentration of ~25 pM in SSPE buffer. 200 μL of this mixture was placed on a bovine serum albumin (BSA)-coated glass coverslip (VWR) and was measured using the cTCCD instrument. The coverslip surface was wiped clean and coated with 1 mg mL^{-1} BSA for 20 min at room temperature to prevent adsorption of the sample protein onto the slide then excess BSA was removed. Between 400 and 600 frames (of 8s of data per frame) were acquired with a bin time of 1 ms, a scanning speed of 200 μm s^{-1} and at a temperature of 21°C (Supplementary Fig. 1).

For TIRFM imaging, the sample was prepared by diluting the desired aliquot of the sample to a concentration of ~40 nM in SSPE buffer and incubating on a cleaned slide for 30 s to 1 min. The slides were pre-cleaned with a piranha solution (3:1 sulfuric acid: hydrogen peroxide) for 1 h and then washed with distilled water. The slides were then imaged using the TIRFM setup and separate color frames were overlaid using Metamorph imaging software (Supplementary Fig. 1).

During each of the disaggregation experiments, 6–7 μM of the Aβ monomer was observed to be incorporated in the fibrils. Over the 48 h disaggregation experiment, about 4% of the material originally present in fibrils disaggregates into monomers or stable oligomers with a ratio of monomers to stable oligomers of approximately 1700:1. This was found to be repeatable—i.e. if the oligomers and monomers were washed away from the fibrils, and the same fibrils were once again incubated, they would regenerate this distribution.

II.   **cTCCD and TIRFM data analysis**

Preliminary data processing

The data analysis for cTCCD measurements was performed as previously described[46]—by first processing the frames for coincident bursts above an intensity count of 10 for each 1 ms bin (in order to exclude background fluorescent signal from

buffers and coatings). In order to account for "chance coincidence" (molecules that are not necessarily associated but that appear simultaneously in the confocal volume), a method called desynchronization was used[47]. Frames are reshuffled so that the nth frame from one detection channel is paired with the n±1 frame from the other detection channel. Any events that appear as coincident after this reshuffling are counted as chance coincident events.

For sets of data where the sample contained lowly-fluorescent but highly scattering material such as dust, frames containing bursts with a signal above 10 counts per bin for at least 10 consecutive bins were removed from the dataset. These criteria were chosen empirically as most effective in eliminating dust particles from previous trials. Such filtering procedures ensured that the data analysis parameters given by single molecule bursts were not biased by dust, buffer impurities or coverslip coating defects to which cTCCD is more sensitive due to the scanning over a large sample area.

For TIRFM images, ImageJ (NIH, freeware) was used in order to determine the length of fibrils. The line-length measurement tool was used to trace over each fibril and each was categorized. This was performed for ~200 fibrils for each set of measurements in order to acquire an adequate sample size.

Determining populations of various species

In order to determine the percentage of oligomers in solution, the number of coincident bursts (oligomeric) was compared to the total number of bursts. This number was corrected for the detection efficiency of the instrument (~25%) as well as for the detection limitations of cTCCD for certain types of oligomers. For example, our cTCCD analysis identifies oligomers from monomers on the criterion of a coincident burst. Therefore, since the cTCCD data analysis software is sensitive to only two-color species, a dimer comprised of two red-labeled or two-blue labeled molecules would not be separable from the monomers and would therefore not be separately detected. However, we can account for this limitation in our data analysis as the detection efficiency limit varies binomially and inversely with oligomer size. The undetected fraction is highest for dimers (0.5) but scales as the binomial probability distribution rendering it below 0.01 for any oligomer over seven monomers in size. Therefore, we know the exact proportion of undetected species for each sized oligomer.

The amount of monomeric sample (non-coincident bursts) was determined using burst-rate counting in a similar way to the oligomeric (coincident burst) counting.

Burst rates were correlated with concentrations using a set of known DNA samples as concentration standards. Any difference between diffusion coefficients for the DNA standard and the Aβ were negligible as the measurements were taken with the probe volume scanning over the sample volume at speeds greater than the diffusion speeds of these molecules (see above section on instrumentation for details).

Estimation of oligomer size by cTCCD

Apparent size distributions were determined by using the burst brightness in the blue channel scaled by the average monomer brightness (over 600 frames) to obtain an effective number of monomers. This number was then doubled to give the average number of monomers in the complex.

Since the $A\beta_{1-40}$ is a small peptide, the oligomers experience a substantial amount of FRET. This affects the brightness of the two channels. A correction to account for the FRET was made by comparing the intensity distribution of events in the blue channel to that of a control non-FRETing but highly coincident sample (40bp dually-labeled duplex DNA). The logarithm of the intensity distribution of coincident events for both the FRETing $A\beta$ oligomers and non-FRETing model DNA samples was plotted. The ratios of the slopes of linear fits of these data were used as a FRET correction factor. The uncorrected sizes were multiplied by this correction factor to obtain the corrected (for FRET) size which we have called apparent size.

Similar calculations of apparent size were performed for the bursts that were coincident by chance only (as determined by the desynchronization approach described earlier) and this distribution of "chance coincident" sizes was subtracted from the distribution of total distribution of "all coincident" sizes to yield the final distribution of "real coincident" apparent sizes.

In order to determine what bin sizes to use for presenting distributions of apparent sizes, we determined the uncertainty in our measurement associated with variation in fluorophore brightness, error in determining the FRET correction factor, and finally the binomial error associated with the assumption that each oligomer contains an equal number of red and blue fluorophores. These errors were empirically or theoretically determined and the relative errors were summed in quadrature to obtain the net uncertainty in the size determination. These relative errors varied from 63% for trimers down to 17% for 50-mers (Supplementary Fig. 3). Dimers had a lower relative error of 30% percent since they do not have any associated binomial error—the criteria of coincidence detection defines a dimer as containing a single blue and single red fluorophore.

Estimation of oligomer size by TIRFM

As a conformation of the cTCCD-based size determination method, TIRFM imaging was also used to estimate the oligomer size distribution. Samples of HiLyteFluor647-labeled $A\beta_{1-40}$ from various stages of aggregation were adsorbed onto piranha-cleaned glass slides and at low-nanomolar concentrations. Images were acquired as previously described. These were then analyzed using custom-written software (MATLAB). Background regions were user-defined by choosing a background area on the slide,

corresponding to a region with no Aβ adsorption. The images were band-pass filtered and the threshold for the subsequent spot detection was determined from background region selected. Detection of spots corresponding to Aβ oligomers was performed using centroid fits to bright objects[48]. Spot intensities corrected for the local background were extracted. These spot intensities were scaled by the average monomer brightness determined in a similar manner for monomeric solutions adsorbed onto glass slides. This oligomer size corresponds well with those measurements made by cTCCD supporting our fluorescence lifetime data (below) as well as previous work which suggests that there are low levels of fluorescence quenching even in higher order oligomers[49].

Curve fitting

The rate of change of soluble species in solution (whether oligomer or monomer) was fit to the following expression: $[S] = A(1 - e^{-k(x-c)})$ which assumes monomolecular dissociation of fibrils into soluble species using Origin 8 software (OriginLab). In this expression S represents soluble species and A represents this equilibrium ratio of species released. The parameter c is a non-zero constant here as it represents the number of pre-existing soluble species that were not removed by washing and k is the rate constant derived for the first order reaction. We assume here that this rate is independent of fibril concentration, i.e. that the rate of disaggregation is an intrinsic property of each fibril.

III.   Fluorescence lifetime imaging of fluorophores

Fluorescence decay traces of HiLyteFluor488 and HiLyteFluor647-labeled Aβ$_{1-40}$ were recorded in Time-Correlated Single Photon Counting (TCSPC) mode using a FluoTime 200 fluorescence lifetime spectrometer (PicoQuant GmbH, Berlin, Germany). The excitation sources were two pulsed lasers with excitation wavelengths of 465 and 632 nm (LDH-P-C-470 and LDH-P-C-635B respectively, PicoQuant GmbH). The repetition rate of 20 MHz for the laser pulses was controlled by a PDL-828 Sepia II driver unit (PicoQuant GmbH). The laser polarization was kept in the vertical plane by a single-mode fiber coupler. Fluorescence was collected beyond a polarizer set at the magic angle and a 2 nm bandwidth monochromator to select the emission wavelength. A TimeHarp 200 PC-board (PicoQuant GmbH) was used to collect the discriminated signal and plot fluorescence decay histograms over 1320 channels with a time increment per channel of 36 ps. TCSPC histograms were recorded until they reached 2×10^4 counts at the maximum. Decay traces were analyzed by a least squares based deconvolution method in terms of multi-exponential functions using FluoFit software (PicoQuant GmbH), employing instrument response functions collected using Ludox scatterer.

For HiLyteFluor488 labeled peptides ten decay traces were collected: two repetitions of the emission wavelengths 515, 525, 535, 545, and 555 nm, with the excitation at

465 nm. For HiLyteFluor647 labeled peptides ten decay traces were collected: two repetitions of the emission wavelengths 665, 670, 675, 680, and 685 nm, with 633 nm excitation wavelength. For mixed fibrils with peptides labeled with both fluorophores six decay traces were collected with 465 nm excitation, at the emission wavelengths 515, 525, 535, 545, 680 and 685 nm, and five emission wavelengths (665, 670, 675, 680, and 685 nm) with excitation at 633 nm. The decay traces collected from each sample were fitted globally with the decay times linked as shared parameters, whereas the pre-exponential factors were local adjustable parameters. The quality of each fit was judged by measuring the reduced χ^2 value and the randomness in the distributions of weighted residuals and autocorrelation functions.

In each case, the mature fibrils were centrifuged and washed (as described in Methods). We analyzed the decay traces from two supernatant solutions of consecutive fibril washings and the resuspended fibrils to check whether there are differences in the fluorophores' lifetimes.

IV. Bulk measurements of fibril formation: thioflavin-T fluorescence assays, transmission electron microscopy, and monomer consumption

The fibril formation processes of both unlabeled and labeled $A\beta_{1-40}$ were compared using thioflavin-T (ThT). The experiment was performed using peptide concentrations of 5 μM (both HiLyteFluor647-labeled and unlabeled), at 37 °C in a 96-well plate (COSTAR) with shaking at 200 rpm. The peptide was incubated with 20 μM ThT in 50 μM phosphate buffered saline (PBS) at pH 7.3. Excitation was performed at 440 nm and fluorescence was monitored at 480 nm (BMG FLUOstar OPTIMA plate reader). Each measurement was done in duplicate or triplicate. The HilyteFluor488-labeled $A\beta_{1-40}$ was not used for this incubation as its own fluorescence overlaps with the fluorescence from ThT.

TEM of labeled and unlabeled fibrils were examined to confirm that the morphology of fibrils formed from labeled-$A\beta_{1-40}$ did not differ from those made from the unlabeled peptide. Formvar-Cu^{2+} grids were exposed to ultraviolet light for 5 min after which 10 μL of the sample solution was placed to adsorb onto the grid for 2 min. Then the sample was blotted off, the grid washed twice with deionized water, and incubated with 10 μL of uranyl acetate (2% w/v) for 2 min to negatively stain the fibrils. The uranyl acetate was then blotted off and the grid was dried and stored at room temperature for subsequent examination under the electron microscope (FEI Philips CM100 TEM).

In order to compare the rate of monomer consumption of the labeled and unlabeled $A\beta_{1-40}$ peptides, aggregation reactions at 2 μM were performed with both peptides. For the unlabeled and labeled peptides, samples of 20 μL at each timepoint were taken, centrifuged in a table-top centrifuge for 10 min at 11,400×g and the supernatant removed. The supernatant was then loaded on a Tris-tricine 7−12% (w/v) acrylamide gel. The labeled protein was first visualized directly on the gel using fluorescence

scanning (Typhoon instruments) and then the unlabeled (and labeled) proteins were detected using Western immunoblotting techniques. To do this, the protein was transferred to a nitrocellulose membrane and was detected using primary anti-Aβ antibodies (6E10) and secondary antibodies by either fluorescence or chemiluminescence (for the labeled protein). The rate of monomer consumption was determined by quantification of the gel bands using ImageJ image analysis software. Additionally, for the labeled peptide, cTCCD measurements were also made throughout the aggregation to compare the results from bulk and single-molecule methodologies.

V. Calculation of thermodynamic values

Using the apparent size distributions at times late during both the aggregation (during the ThT-plateau phase) and the disaggregation experiments (after stabilization of total species concentration), we calculated equilibrium constants for the addition of a monomer to a species of apparent size n−1 (where n−1 varied from 1 to 49).

$$(A\beta)_{n-1} + (A\beta)_1 \rightarrow (A\beta)_n$$
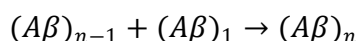
Using the concentrations for monomers and various sized oligomers at these points, the equilibrium constants were calculated for each species from dimer (K_2) to 50-mer (K_{50}) using the following expression.

$$K_n = \frac{[(A\beta)_n]}{[(A\beta)_1][(A\beta)_{n-1}]}$$

Using this equilibrium constant, the standard free energy of formation (ΔG°) for various sized species via monomer addition can be determined in both aggregation and disaggregation reactions using the following equation.

$$\Delta G_n^{\circ} = -\text{RT} \ln(K_n)$$

In order to determine entropic and enthalpic contributions to the ΔG° value, a temperature dependent study was done using the disaggregation experiment. It was performed at three different temperatures (310 K (37 °C), 294 K (21 °C), and 277 K (4 °C)) and the apparent size distributions were calculated and equilibrium constants were extracted as above. Using the temperature and equilibrium constants in the van't Hoff relationship, the standard enthalpy and entropy of formation of various sized oligomers were determined.

$$\ln(K_n) = -\frac{\Delta H_n^{\circ}}{RT} + \frac{\Delta S_n^{\circ}}{R}$$

VI. Protocols for experiments with clusterin

Labeling of clusterin with AlexaFluor647

Clusterin was extracted from human serum from Wollongong Hospital (Wollongong, NSW, Australia), as described previously[50]. Labeling of the protein was conducted at a protein concentration of 70 μM at cysteine residues using a maleimide-linked AlexaFluor647. The pH of the reaction mixture was adjusted to 8.3 using 100 mM $NaHCO_3$ and the dye was then dissolved in the protein solution at a 20 times excess and left to react with agitation for 2 h at room temperature. The reaction mixture was quenched with Tris base and diluted to a total reaction volume of 500 μL. Free dye was removed from the reaction mixture using two sequential 5 mL HiTrap Desalting columns (GE Life Sciences). A monoQ ion exchange column (GE Healthcare) was used to separate unlabeled from labeled protein by eluting over a salt gradient from 1−100% (w/v) $NaHCO_3$ with 1M NaCl over 60 column volumes. The final yield of labeled protein was 4%. Concentration of labeled protein was determined using the burst rate calculated from cTCCD measurements.

Protocols for cTCCD experiments with clusterin

In order to investigate which $A\beta_{1-40}$ species (monomers or oligomers) in the forward reaction were bound to clusterin, we used AlexaFluor647-labeled clusterin and incubated this at a 1:1 molar ratio with aliquots from an aggregating solution of HiLyteFluor488-labeled $A\beta_{1-40}$. These experiments were performed at 2 μM Aβ and clusterin. The samples were then diluted to ~25 pM for analysis by cTCCD.

For the fibril disaggregation experiments, $A\beta_{1-40}$ fibrils were formed in the absence of clusterin at 8 μM, 37 °C in SSPE buffer. After 72−96 h, a time by which mature fibrils were formed, equimolar amounts of clusterin were added to the incubation mixture and the mixture was incubated for 12−16 h at room temperature. The fibrillar pellet (65 ± 5% of the original $A\beta_{1-40}$ remained in the fibrillar pellet) was then separated from the soluble material by centrifuging the pellet and resuspending it in fresh buffer solution as in the fibril disaggregation experiments performed in the absence of clusterin. Only 0.2−0.7 μM of clusterin remained associated with the fibrillar pellet and of that, ~90 nM of the clusterin dissociated from the fibrils over the course of the disaggregation reaction. The species released into the solution were monitored by cTCCD. Alternate control experiments were performed without the 12−16 h of incubation with clusterin but rather by just adding in soluble clusterin with the buffer above the fibrillar pellet. Additionally, control experiments were performed using unlabeled lysozyme instead of clusterin to ensure observations were specific to clusterin.

The above experiments were performed with unlabeled clusterin (and a 1:1 mixture of HiLyteFluor488 and HiLyteFluor647-labeled $A\beta_{1-40}$ peptides) to observe the effects of clusterin on the oligomer distributions. They were subsequently performed using AlexaFluor647-labeled clusterin (and only HiLyteFluor488-labeled $A\beta_{1-40}$) to detect clusterin:Aβ complexes.

In order to study the stability of clusterin:oligomer complexes, solutions containing these complexes were diluted from original aggregation or disaggregation reactions 100−200 fold and incubated at room temperature for approximately 50 h. The resulting concentration of these solutions was in the picomolar to nanomolar range (total peptide concentration of ~10 nM for disaggregation experiments and between 50 pM and 20 nM for aggregation experiments). Complex dissociation was monitored by measuring the change in fraction of associated species with time by cTCCD.

Supplementary Discussion

VII. Fluorescence lifetime measurements

Three different lifetimes were obtained for oligomers and fibrils from HiLyteFluor488-labeled $A\beta_{1-40}$. The predominant component (>80%) in the supernatant solutions showed a lifetime of 3.99 ± 0.01 ns that corresponded to the unquenched fluorophore. The dye HiLyteFluor488 is reported to have a fluorescence lifetime of 4.1 ns[51]; therefore this confirmed that the fluorophore is not quenched when attached to the $A\beta_{1-40}$ peptide. The decay traces showed however two other components with lifetimes of 1.41 ± 0.08 and 0.13 ± 0.01 ns respectively. These represent quenched fluorophores caused by homo-FRET or self-absorption in high-order oligomers, protofibrils and fibrils. The shortest decay time of 0.13 ns is the predominant component in the resuspended fibrils, which suggests that this is the fluorophore lifetime within the fibril. The intermediate lifetime of 1.41 ns must correspond to high-order oligomers in which the packing of the monomers is not as tight as in the mature fibrils.

The decays of the HiLyteFluor647 fluorophore are more difficult to interpret because the fluorophore itself presents multi-exponential decays, as is common with cyanine-type dyes. The lifetime of the free HiLyteFluor647 dye is 1.0 ns[51]. 100% of HiLyteFluor647-labeled $A\beta_{1-40}$ in the supernatant solutions was a mixture in equilibrium of components with two decay times, in which the principal material is monomeric protein or small oligomers. The decay times were 1.77 ± 0.03 and 1.12 ± 0.01 ns, showing an average lifetime of 1.30 ± 0.02 ns. In the HiLyteFluor647-labeled, resuspended fibrils a third lifetime component of 0.11 ± 0.01 ns appeared, which could also corresponding to highly quenched fluorophores within tightly-packed fibrils.

These features were maintained in the case of fibrils grown with a mixture of HiLyteFluor488 and HiLyteFluor647-labeled proteins. The only appreciable difference is that the short lifetimes of HiLyteFluor488 were 1.30 ± 0.10 and 0.07 ± 0.01 ns. This means an additional decrease in the lifetimes probably due to a more effective quenching caused by FRET to the acceptor dye (HiLyteFluor647) within the higher-order oligomers and fibrils.

VIII. Fluorescent dyes do not affect $A\beta_{1-40}$ aggregation

In order to confirm that the labeling of $A\beta_{1-40}$ with HiLyteFluor fluorophores did not affect the behavior of the peptide, the rates of fibril formation for both labeled and unlabeled peptides were tracked using ThT fluorescence. The experiment was performed in either duplicate or triplicate at concentrations of 5 μM and 1.7 μM with both unlabeled and HiLyteFluor647-labeled $A\beta_{1-40}$ both prepared as described earlier. HiLyteFluor488-labeled $A\beta_{1-40}$ was not used since its absorbance and emission

properties would interfere with those of ThT. Both unlabeled and labeled 5 μM ThT traces have similar growth profiles and times (Supplementary Fig. 2a). Since the fluorophore-labeled Aβ$_{1-40}$ exhibits similar behavior to its unlabeled counterpart, the attachment of the dye is assumed to have little effect on the aggregation of the peptide.

Additionally, the fibril morphology (examined by TEM) of the HiLyteFluor488 and HiLyteFluor647 mixed-fluorophore fibrils were similar to those comprised of unlabeled Aβ$_{1-40}$ further supporting that fluorophore labeling does not perturb the aggregation products (Supplementary Fig. 2b).

Finally, we found good agreement between the rates of monomer consumption measured by the burst rate decrease in single molecule measurements and by the decrease in intensity of the soluble Aβ fraction on a western blot (using primary antibody 6E10 against Aβ and secondary antibodies with chemiluminescent and fluorescent properties) which further supported that labeling of the peptides did not affect the peptides' aggregation process (Supplementary Fig. 2c). We also found that the HiLyteFluor488 and HiLyteFluor647-labeled peptides were incorporated into fibrils at equal rates in single-molecule experiments confirming that there was no preference towards aggregation of one color of peptide (Supplementary Fig. 2d).

IX.   cTCCD is capable of detecting small quantities of soluble aggregates

In order to confirm that the small percentages of oligomers observed were, in fact, real signs of aggregation, we compared a typical aggregation trace to one taken with Aβ$_{1-40}$ under non-aggregating conditions (i.e. pH 11.5, where the peptide is monomeric). We observed a distinguishable difference between these traces which indicated that we could detect aggregation (Supplementary Fig. 3a). This shows that even though there is a low population of aggregates, it is beyond the noise of the measurement.

X.   Single molecule apparent size distributions represent those present at bulk conditions

We quantified the effects of the ~10,000-fold dilutions required for single molecule measurements on labeled oligomeric Aβ$_{1-40}$ samples (at 2 μM with ~1% oligomer concentration) by performing cTCCD measurements and instead of diluting them into buffer, diluting into a solution of unlabeled Aβ$_{1-40}$ so that the total Aβ concentration remained at 2 μM while the concentration of labeled protein was decreased to single-molecule (pM) concentrations. This did not affect the measurement capability as the unlabeled Aβ is invisible to cTCCD. This experiment revealed that the 10,000-fold dilution step caused a ~50% decrease in overall oligomer concentration but no alteration in the distribution of apparent sizes (see Supplementary Fig. 3b). These oligomers had an apparent size distribution that was similar to those measured from the same sample diluted into a buffer without unlabeled Aβ. Therefore, we suggest that although dilution does destabilize approximately half of the oligomers, the oligomers

observed at single-molecule concentrations are representative of the total oligomeric population.

XI. Distribution of oligomer sizes remains constant with time

Observing the apparent size distributions (calculated as mentioned in the Supplementary Methods) for an aggregation reaction revealed no major changes in the exponential-type distribution as the reaction proceeded (Supplementary Fig. 3c).

XII. Estimation of oligomer sizes and associated errors using TIRFM is similar to that obtained by cTCCD

The error associated with oligomer size determination by cTCCD was calculated as described in Methods (Supplementary Fig. 3d).

In order to confirm that our cTCCD-based estimation of "apparent oligomer size" was valid across multiple methods, we used TIRFM to estimate the sized distribution of soluble oligomers. Using this, we found a good correlation between the size distribution estimated by TIRFM and that determined by cTCCD (Supplementary Fig. 3e). Since TIRFM measurements are performed with a single color and with immobilized species, they validate the method used to determine size using brightness data from cTCCD.

XIII. Fluorescent labeling of clusterin does not affect its activity

In order to confirm that labeling clusterin with AlexaFluor647 did not affect its behavior, we compared the effects labeled and unlabeled clusterin had on the disaggregation. The rate of release of species into solution was very similar for the disaggregation in the presence of labeled (($1.8 \pm 0.6)\times10^{-5}$ s^{-1} n=4, s.d.) and unlabeled (($3.1 \pm 2.1)\times10^{-5}$ s^{-1} n=3, s.d.) (Supplementary Fig. 4a). The difference between the two rates is not statistically significant (with a P-value of >0.99, two-sample independent, two-tailed t-test).

XIV. Clusterin binds oligomers formed at both 100 nM and 2 μM Aβ$_{1-40}$ to form very long-lived complexes

In order to observe clusterin action under multiple incubation conditions, we performed an aggregation at 100 nM total Aβ$_{1-40}$ peptide concentration where there is a considerable lag phase in the formation of fibrils. Oligomers are still observed to form at these concentrations and these oligomers, when incubated with a 1:1 molar ratio of AlexaFluor647-labeled clusterin, were observed to form long-lived clusterin:Aβ complexes. The differences between the fraction of Aβ species in

oligomeric assemblies ($(1.2 \pm 0.7) \times 10^{-3}$) and the fraction of Aβ in clusterin:Aβ complexes ($(1.7 \pm 0.8) \times 10^{-3}$) was not significant (n= 8, P-value of 0.35 in a paired, two-tailed t-test, and P-value of 0.2 for comparison of means in a two-sample independent, two-tailed t-test) (Supplementary Fig. 4b). This suggests that clusterin acts similarly on these species as it does on those formed at higher concentrations—by binding and sequestering any oligomers present.

Additionally, the size distributions of the species formed at 100 nM in the absence and presence of clusterin were remarkably similar to each other and to those formed at 2 µM Aβ$_{1-40}$ (Supplementary Fig. 4c) further supporting that clusterin acts similarly on oligomers formed during an incubation with an extended lag phase as on those formed in a solution that forms fibrils quickly.

Finally, these complexes were found to persist at concentrations as low as 50 pM for over 200 h of measurement with no detectable dissociation suggesting that these complexes, like those formed during aggregation reactions without a lag phase, are extremely long-lived (Supplementary Fig. 4d).

XV.   Stoichiometry of clusterin:Aβ complexes

Using the apparent size metric derived from fluorophore brightness, we can determine the approximate stoichiometry of clusterin:Aβ in the long-lived complexes. The median ratio of clusterin:Aβ in these complexes is 1:15 ± 1.1 (IQR) (Supplementary Fig. 5a). We can also look at the mean ratios of clusterin:Aβ for different sizes of Aβ oligomers and we can see that mean size varies between 1.9 ± 0.02 and 5 ± 1.8 (Supplementary Fig. 5b). The differences between these ratios are not statistically significant with a P-value of 0.25 (ANOVA single-factor test). Therefore, we could attribute this variation to random association of clusterin molecules to each other as they have a tendency to self-associate.

## XVI.   Pre-binding to fibrils is not necessary for observing effects of clusterin

It was confirmed that incubating of Aβ$_{1-40}$ fibrils overnight with clusterin was not necessary to observe the effects of clusterin in suppressing disaggregation. The addition of soluble clusterin also results in a reduction of the extent of monomer disaggregation from the Aβ$_{1-40}$ fibrillar pellet as well as increased oligomer disaggregation, the same effects that were observed in the experiments with pre-binding of the clusterin to fibrils for 12−16 h. However, the magnitude of these effects observed in the two experiments does vary (Supplementary Fig. 6). This can be most likely attributed to the difference in the concentration of soluble clusterin between the two experiments. In the experiment with soluble clusterin without pre-binding, the clusterin concentration is ~8 µM. Whereas, in the experiment with pre-binding of clusterin, most of the soluble clusterin is removed (> 7 µM) and the clusterin that remains is either bound to fibrils (0.2−0.7 µM) or released over the course of the

disaggregation process into solution to yield a final soluble clusterin concentration of ~100 nM. Therefore, it is understandable that there is an observed increase in stabilized oligomer population in the experiment with soluble clusterin as opposed to the experiment with pre-binding to the fibrils, as the concentration of soluble clusterin is over an order of magnitude higher in the former experiment. It is striking to note that even with a greater than 1000% increase in the amount of soluble clusterin (with the soluble clusterin disaggregation experiment) there is only a ~300% increase in the concentration of oligomers stabilized which could suggest that at this point, with an excess of clusterin, we have stabilized most of the oligomers. It was not possible to perform these experiments with labeled clusterin as the detection efficiency of complexes would be compromised due to the severe concentration difference between the clusterin in solution (μM) and the Aβ_{1-40} released into solution (nM).
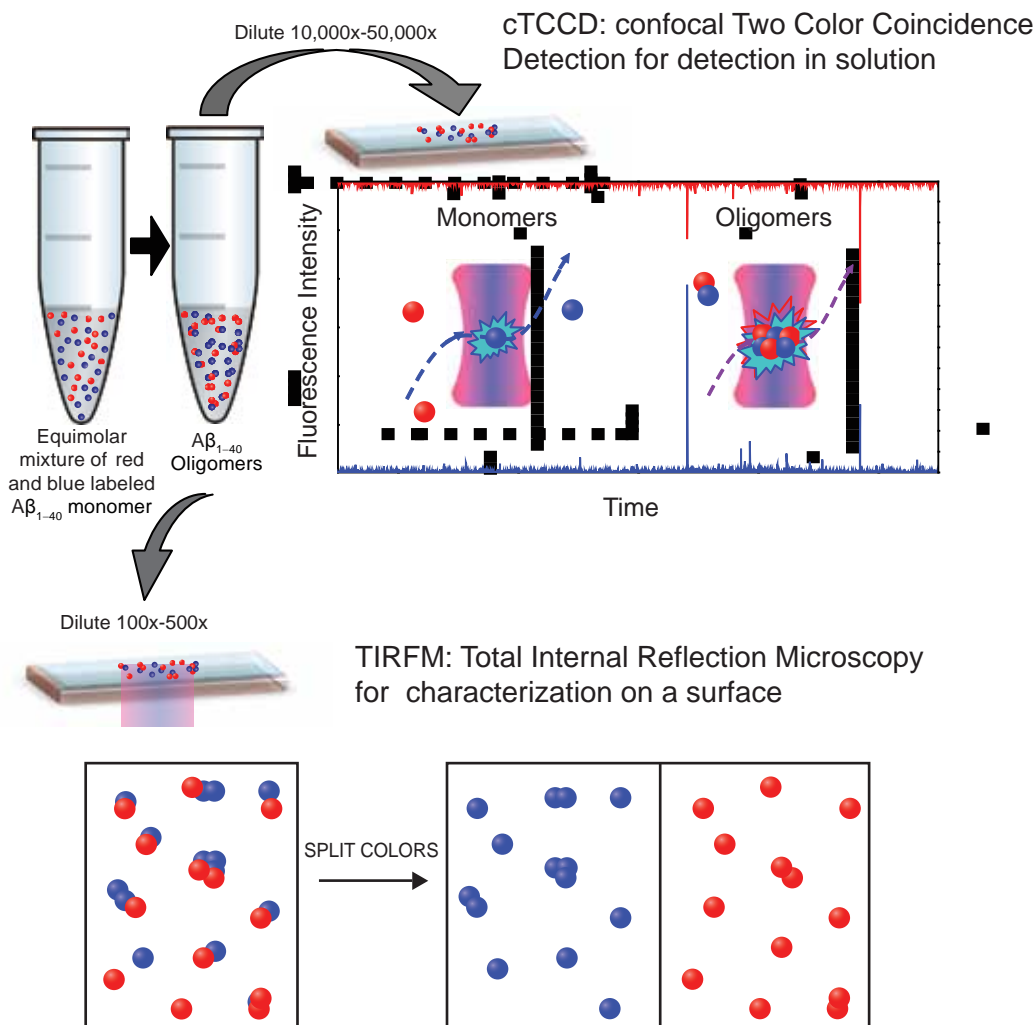
Supplementary Figure 1 cTCCD and TIRFM methods for analyzing amyloidogenic samples. For aggregation experiments, equimolar mixtures of HiLyteFluor488 and HiLyteFluor647-labeled $A\beta_{1-40}$ monomers were combined and allowed to aggregate. Over the course of the aggregation reaction, samples were taken from the mixture and diluted for cTCCD and TIRFM analysis. For TIRFM analysis, a larger area of the slide was dually excited to image multiple $A\beta_{1-40}$ species simultaneously. In both cases, the intensity of the bursts correlate with the apparent size of the oligomer.
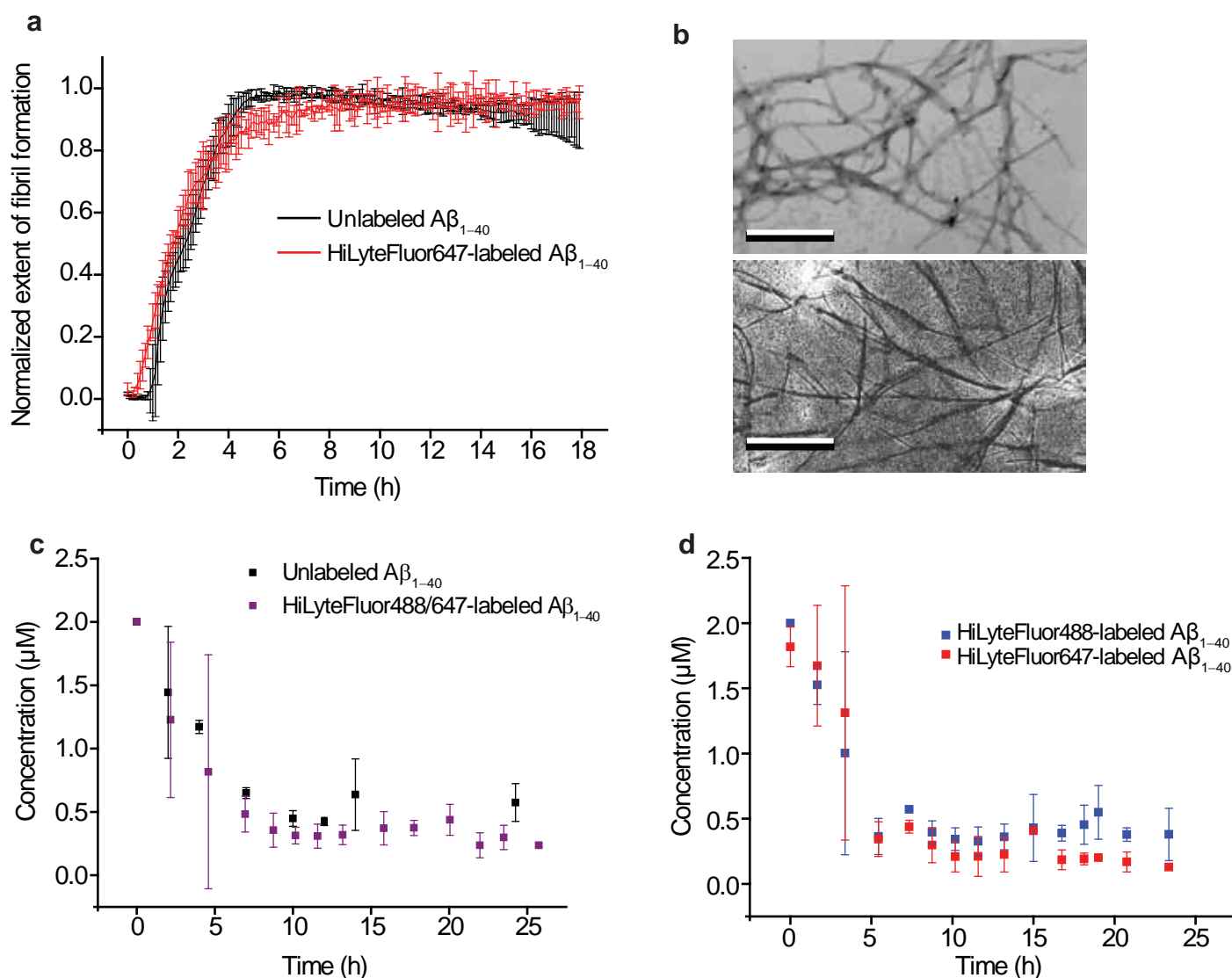
Supplementary Figure 2 Comparison of aggregation of unlabeled and labeled $A\beta_{1-40}$. (**a**) Normalized traces tracking fibril formation for labeled and unlabeled peptide via increase of fluorescence of Thioflavin-T. Only the HiLyteFluor647-$A\beta_{1-40}$ peptide is used as the HiLyteFluor488 fluorophore interferes with the measurement of ThT fluorescence (error bars are $2 \times$ s.d., 5 µM, n=3). (**b**) Transmission electron microscopy (TEM) images of fibrils made from a 1:1 mixture of HiLyteFluor488-labeled and HiLyteFluor647-labeled $A\beta_{1-40}$ (top) and unlabeled (bottom) $A\beta_{1-40}$ peptides. Scale bars are 200 nm. (**c**) A comparison of the rates of decrease in monomer concentration between labeled (both HiLyteFluor488-labeled and HiLyteFluor647-labeled $A\beta_{1-40}$) and unlabeled $A\beta_{1-40}$ peptide. The measurements on unlabeled peptide were performed using western blot band densitometric quantification while measurements on labeled peptide were performed using both western blot densitometry and cTCCD (error bars are s.d., range, $[A\beta_{1-40}]=$ 2 µM, n=3 labeled, n=2 unlabeled). (**d**) A comparison of the rates of decrease in monomer concentration between the two flurophore-labeled forms of $A\beta_{1-40}$ tracked using single molecule cTCCD (error bars are s.d., $[A\beta_{1-40}]=2$ µM, n=3 for both).
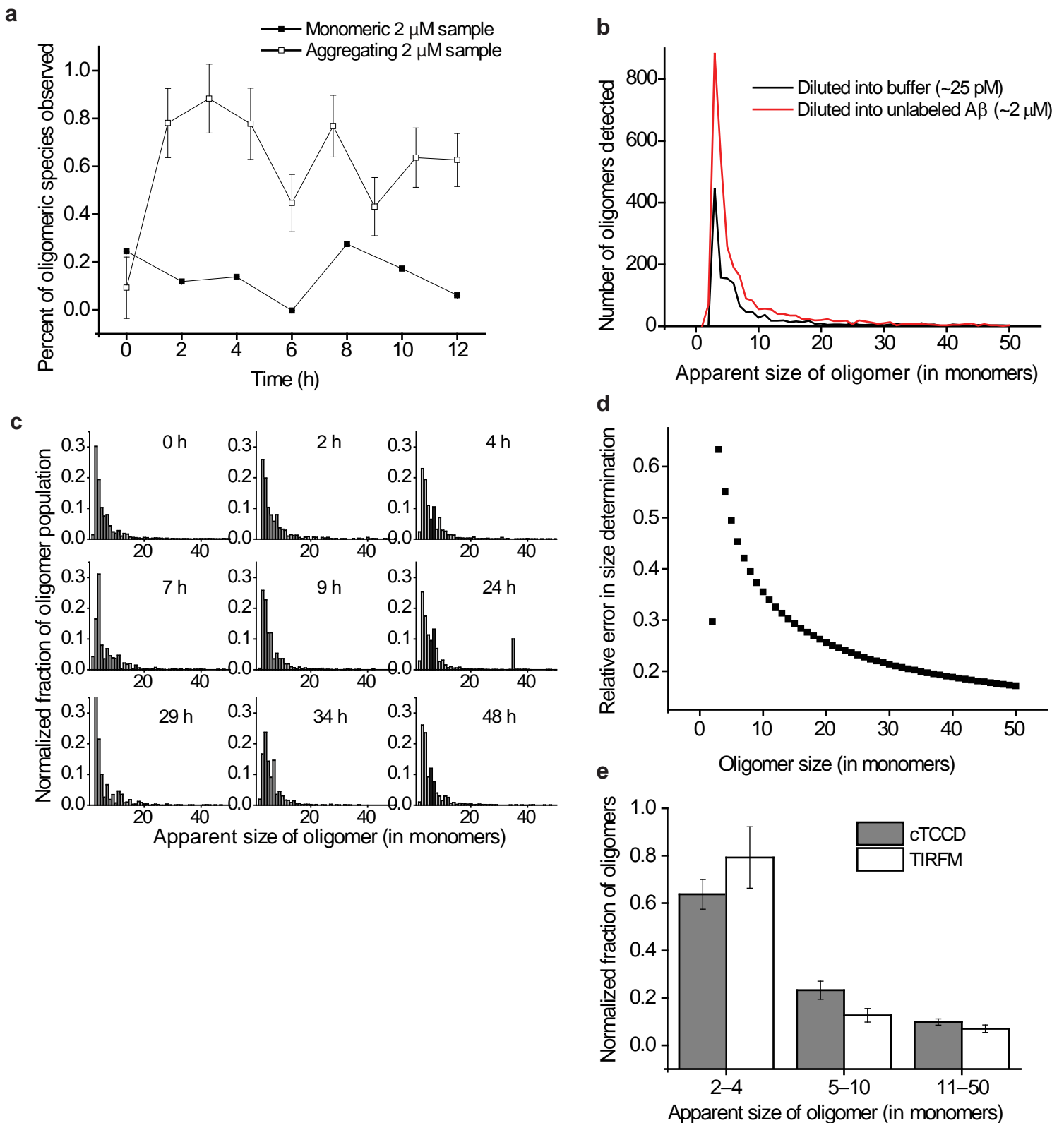
Supplementary Figure 3 cTCCD can characterize oligomers formed during $A\beta_{1-40}$ aggregation. (**a**) A comparison of the percent of oligomeric $A\beta_{1-40}$ species observed in an aggregating sample and a non-aggregating monomeric sample (error bars are s.d.). Error bars for monomeric trace are too small to be visible. (**b**) Representative distributions of apparent sizes derived from single molecule measurements performed at a total $A\beta$ concentration of 25 pM and 2 μM. (**c**) Distributions of apparent sizes were derived from timepoints over 48 h of a 600 nM aggregation reaction of $A\beta_{1-40}$. At each time, a measurement was taken by diluting the 600 nM aggregating solution to ~25 pM and subsequently analyzing by cTCCD. By 48 h at 600 nM, fibrils were observed by transmission electron microscopy. (**d**) Variation in relative error in apparent size derived empirically from the propagation of consistituent errors. Relative error in dimer size determination is lower than those of similarly-sized oligomers because all dimers detected are of a defined composition (containing a single blue and a single red fluorophore). (**e**) Distributions of apparent size derived from single molecule experiments performed using cTCCD and TIRFM methods (error bars are s.d., n=3).
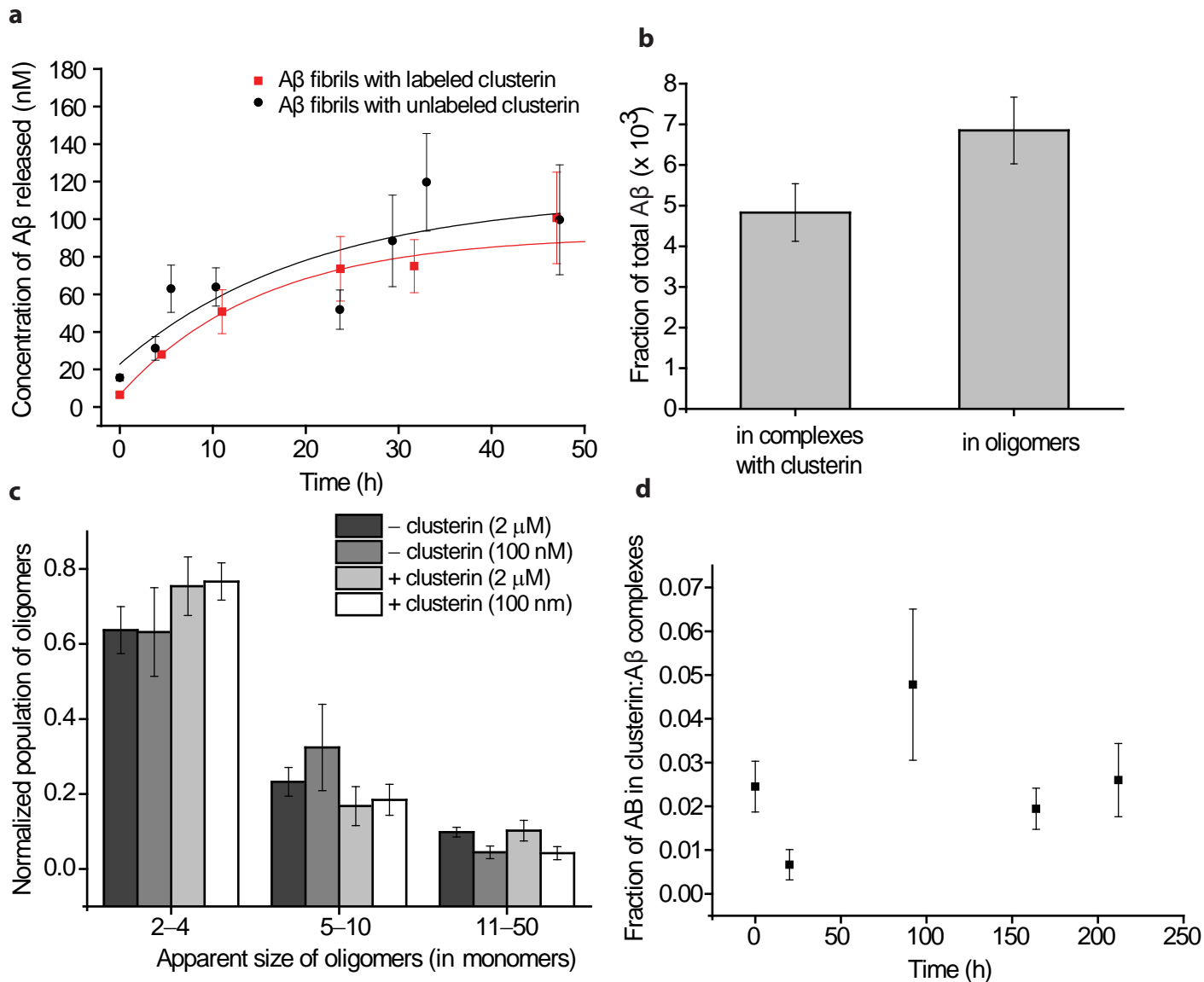
Supplementary Figure 4 Clusterin binds to oligomers formed at 100 nM $A\beta_{1-40}$ concentration in a similar manner to those formed at 2 µM. (**a**) Plot showing the rate of species release into solution (both oligomer and monomer) from fibrils incubated with unlabeled clusterin (black) or labeled clusterin (red). For trials with unlabeled clusterin n=5 (errors are s.e.m.) and for trials with labeled clusterin n=2 (errors are range). (**b**) A plot of the fraction of total $A\beta_{1-40}$ found in oligomeric assemblies and found in Aβ:clusterin complexes at a total $A\beta_{1-40}$ concentration of 100 nM (error bars are s.d., n= 8, P-value of 0.35 in a paired, two-tailed t-test, and P-value of 0.2 for comparison of means in a two-sample independent, two-tailed t-test). (**c**) Distributions of apparent size of oligomers bound to clusterin and those formed in the absence of clusterin at 100 nM and 2 µM $A\beta_{1-40}$ concentrations (for 100 nM, n=11, for 2 µM, n=3, error bars are s.e.m.). (**d**) Fraction of clusterin:Aβ complexes persisting at 50 pM total peptide concentration at 21 °C. Complexes were formed between clusterin and $A\beta_{1-40}$ oligomers from aggregation reactions performed at 100 nM $A\beta_{1-40}$ and clusterin added at a 1:1 molar ratio (n=2, error bars are range). Differences between timepoints are not statistically significant (ANOVA, single factor, P-value = 0.8).

a

b
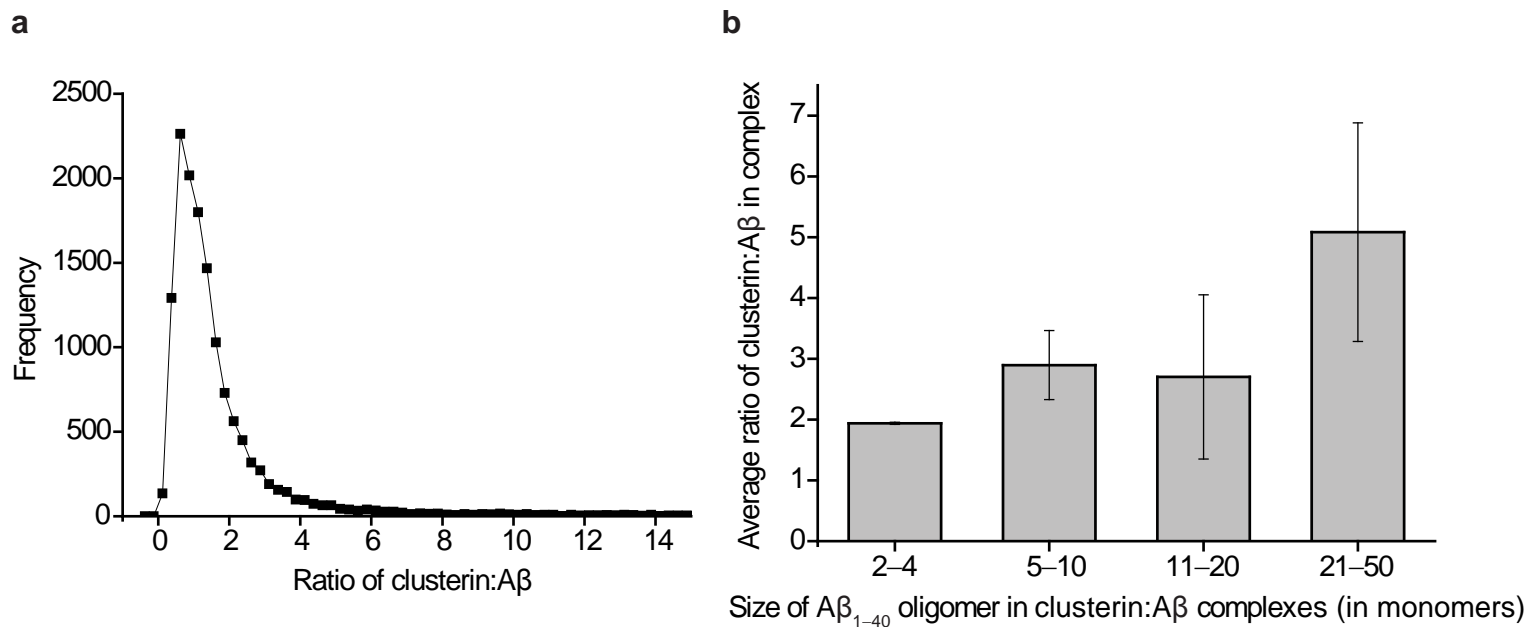
Supplementary Figure 5 Stoichiometry of clusterin:Aβ within complexes is approximately 1:1. (**a**) A histogram of the ratio of clusterin:Aβ in clusterin:Aβ complexes detected by cTCCD. This histogram is compiled from n=3 trials and represents a total of 13,912 complexes analyzed. This indicates that the median ratio of clusterin:Aβ is 1.2 ± 1.1 (IQR). (**b**) A plot of average clusterin:Aβ ratio for for a subset of clusterin:Aβ complexes containing Aβ oligomers with apparent sizes of dimers−50-mers (n=3, error bars are s.e.m.). Variation in mean ratios is not significant (P-value = 0.25, ANOVA single-factor).
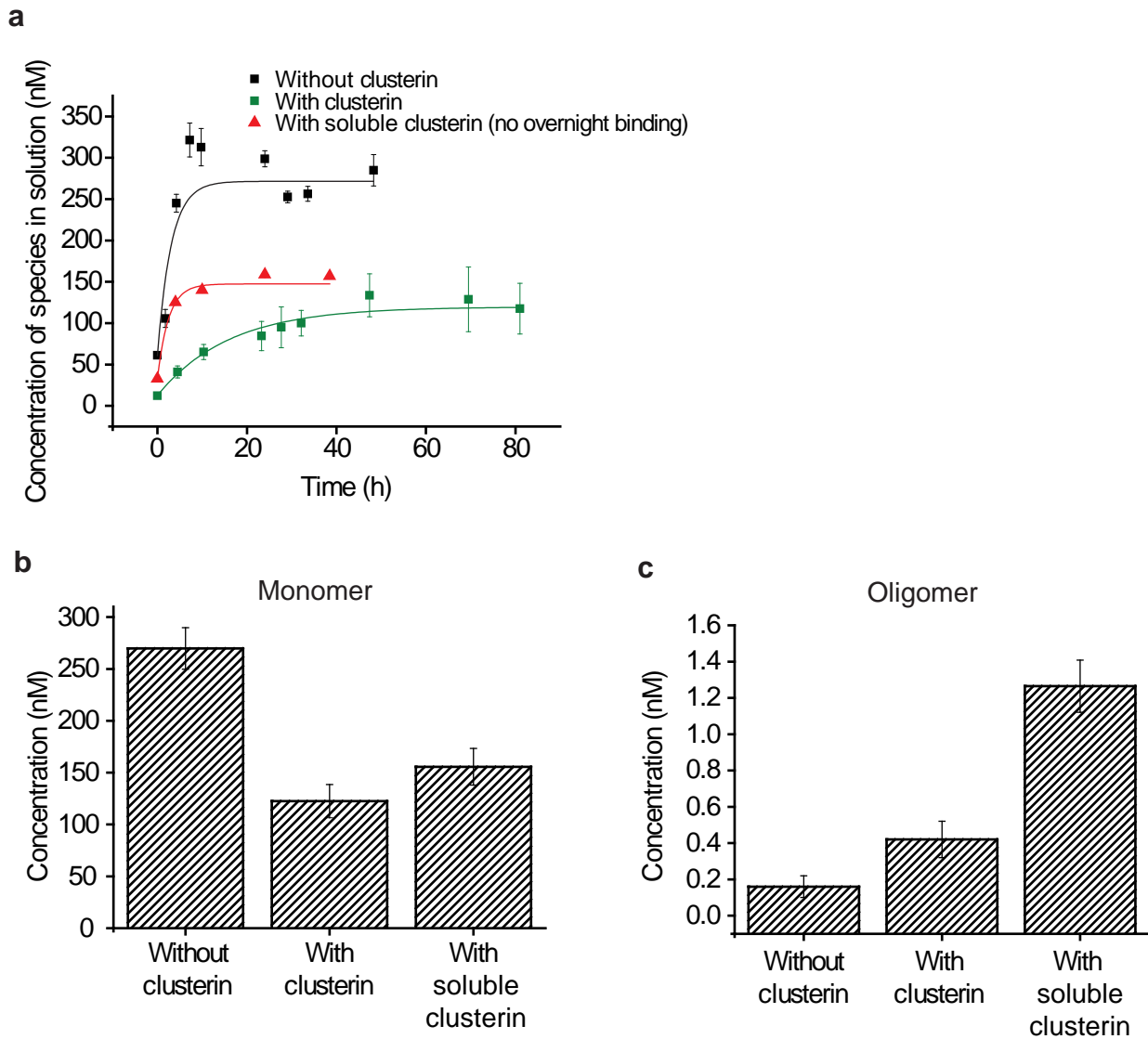
Supplementary Figure 6 Addition of clusterin to $A\beta_{1-40}$ fibrils without pre-binding has similar effects to incubation of clusterin with fibrils for 12 h. (**a**) A plot of the release of species (monomeric and oligomeric) into solution with time for the disaggregation experiment performed in the absence of clusterin (black), in the presence of clusterin in the buffer above the fibrillar pellet (red), and with clusterin bound for 12-16 h to the fibrils (green). Species concentrations were determined by TCCD burst rate analysis on a sample from the buffer above the fibrillar pellet. (**b**) Plots of the monomeric concentration after 50 h of a disaggregation experiment—at this point the relative species concentrations were not observed to change. (**c**) Plots of the oligomeric concentration after 50 h of a disaggregation experiment. For all plots n=12 (without clusterin), n=3 (with pre-binding of clusterin) and n=1 (soluble clusterin without pre-binding). Error bars are s.e.m. in all cases.

References

45. Li, H., Ying, L., Green, J.J., Balasubramanian, S. & Klenerman, D. Ultrasensitive coincidence fluorescence detection of single DNA molecules. *Analytical Chemistry* **75**, 1664−1670 (2003).
46. Orte, A. et al. Direct characterization of amyloidogenic oligomers by single-molecule fluorescence. *Proceedings of the National Academy of Sciences of the United States of America* **105**, 14424−14429 (2008).
47. Orte, A., Clarke, R., Balasubramanian, S. & Klenerman, D. Determination of the fraction and stoichiometry of femtomolar levels of biomolecular complexes in an excess of monomer using single-molecule, two-color coincidence detection. *Analytical Chemistry* **78**, 7707−7715 (2006).
48. Crocker, J.C. Methods of digital video microscopy for colloidal studies. *Journal of colloid and interface science* **179**, 298 (1996).
49. Schauerte, J.A. et al. Simultaneous single-molecule fluorescence and conductivity studies reveal distinct classes of Aβ species on lipid bilayers. *Biochemistry* (2010).
50. Wilson, M.R. & Easterbrook-Smith, S.B. Clusterin binds by a multivalent mechanism to the Fc and Fab regions of IgG. *Biochimica et Biophysica Acta (BBA) - Protein Structure and Molecular Enzymology* **1159**, 319−326 (1992).
51. Anaspec. HiLyteFluor Dyes−Brilliant. 2 (Freemont, CA).